SN Computer Science (2023) 4:228
https://doi.org/10.1007/s42979-023-01701-8

ORIGINAL RESEARCH

Skin Cancer Segmentation Based on Triangular Intuitionistic Fuzzy Sets

Anupama Namburu[1] · Senthilkumar Mohan[2] · Sibi Chakkaravarthy[1] · Prabha Selvaraj[1]

Received: 12 January 2022 / Accepted: 20 January 2023

Abstract
Malignant Melanoma is a dangerous form of skin cancer, and its detection is a challenging task as it appears in numerous ranges of size, shape, and shading with various skin tones. Also, artefacts like hairs, outlines, blood vessels, and boils add further complexity. A simplified clustering method is proposed in this paper to improve melanoma detection while reducing time complexity.The triangular membership function (TMF) is used to detect the initial regions for obtaining initial centroids. These initial centroids are used to apply intuitionistic fuzzy c-means clustering. The TMF helps in identifying the initial clusters and regions and reduces the number of iterations needed for segmentation. The proposed method effectively detects skin cancer regions with an average accuracy of 90% and performs well.

Keywords Fuzzy sets · Intuitionistic fuzzy sets · Medical image segmentation · Image processing · Skin cancer

Introduction

According to the World Health Organization, skin cancer is one of the most common types of cancer worldwide. It ranks 19th among all diseases in men and women, with 324,635 cases reported in the year 2020. With the increased cases, early detection and timely treatment for melanoma are critical for patient survival.

Dermoscopy is a well-known in vivo unobtrusive imaging tool that uses captivated light to help dermatologists inspect pigmented skin sores based on a variety of morphological highlights. In spite of the fact that dermoscopy has been shown to prompt expanded demonstrative exactness, appropriate understanding of dermoscopic images is typically tedious, complex, and costly and depends on the observer's perception. The traditional approaches are carried out with low-quality image processing methods that fall under image analysis in the medical field. The initial methods carried out in cleaning the raw data are done by pre-processing methods that adjust the intensity, contract, redundant data, scaling, and binarisation [1, 2] in the morphological structure of the image.

Recent advances in information technology have resulted in high-performance results in detecting and diagnosing various types of cancer, particularly skin cancer. The unwanted noises are removed with pre-processing methods proposed by [3]. The quality of the image is enhanced by pre-processing methods, which reduce the processing time and complexity.

Image resizing plays an important role while processing the data. As different datasets have varied sizes of images, it is necessary to resize them to the same size to apply the algorithms. The pre-processing is followed by image segmentation to detect the region of interest (ROI). The ROI may be anything that we need to analyze. In the medical image, ROI could be the diseased region that is separated by the unaffected region [4]. This segments the unaffected tissue, and then the required features are considered from the affected region so that the result will be accurate and clear [5].

The classical way of segmenting is performed by thresholding, clustering, and other edge detection methods, and the ABCDE method is used to diagnose melanoma in the

This article is part of the topical collection "Advances in Applied Image Processing and Pattern Recognition" guest edited by KC Santosh.

✉ Anupama Namburu
namburi.anupama@vitap.ac.in

[1] School of Computer Science Engineering, VIT-AP University, Amaravati, Guntur 522237, Andhra Pradesh, India

[2] School of Information Technology and Engineering, Vellore Institute of Technology, Vellore, Tamilnadu, India

Published online: 22 February 2023

skin during the analysis [6]. Even though many methods are incorporated in detecting and diagnosing cancer, there are still many challenges in dealing with real-time image data. It contained many unexpectedly complex data points, and the image's ocular emergence in the affected skin area made separating the desired ROI of melanoma with an accurate contour measure from the image difficult. [7].

Automated state-of-the-art techniques have been developed to help dermatologists improve their effectiveness and objectivity in the visual understanding of dermoscopic images[8]. Automatic image segmentation is performed mainly using classification and clustering. Classification is supervised segmentation that requires prior information about the classes to be classified. Clustering is preferred because it is unsupervised and does not require prior information. However, clustering algorithms require initial centroids to obtain clusters. Wrongly chosen clusters can result in local minima producing invalid segmentation regions, deeming the effort unfruitful.

Many researchers proposed automated methods to overcome these challenges. The broad category of these methods includes thresholding, clustering, classification, and contours and snakes, each having its merits and demerits [9].

Skin lesion segmentation based on thresholding namely, Otsu's[10], fuzzy logic [11], adaptive thresholding [12] are available in literature. The threshold methods lead to irregular edges with varied thresholds. The lesions of a melanoma tend to have fuzzy borders and irregular shapes, leading to uncertainty in identifying the exact lesion from skin images. Researchers have used fuzzy sets and rough sets to address the uncertainty and vagueness in the image. Skin cancer with fuzzy logic approaches are proposed in [13–16]. Fuzzy-based methods have the advantage of representing the intermediate data in intervals, allowing qualitative analysis of the data [3]. A fuzzy intensity threshold with type2 fuzzy logic proposed in [11] was able to detect the pixel intensity either belongs to ROI or the background. These fuzzy-based methods failed to group lesion pixels with low contrast as lesions.

Garcia et al. used fuzzy classification of pixels and histogram threshold with innovative methods applied on skin images for segmentation in [17]. The method used Otsu's threshold with fuzzified regions determination and applied morphological operators to extract the tissues in case of artefacts. Castillejos et al. [14] presented predefined cluster selection using fuzzy c-means. This work specifies automatically, the number of clusters needed by an image for segmentation. The clustering algorithms are highly influenced by the initial centroids and the number of clusters needed for clustering.

Many algorithms based on active contours and snakes are proposed for skin lesion segmentation [18–23]. These algorithms usually depend on the initial curves and positioning of curves that undergo deformation to detect the boundaries of lesions. An automated method for adapting the contour to skin lesions is proposed in [23], but still, the contour selection is needed.

In recent days, many deep learning models for segmenting skin lesions are proposed in the literature based on convolutional neural networks, generative adversarial models [24, 25], deep autoencoders, stacked autoencoders, convolutional autoencoders, restricted Boltzmann's machine, and recurrent neural nets are reviewed and analyzed in [26–31]. Deep learning methods have the ability to obtain the features from images that are useful in segmentation. The performance of the deep learning models has improved when compared to existing methods. However, Graphics Processing Units (GPU) are used in parallel to analyze the features and to detect the skin lesions[8, 32, 33].

Adrian et al. use the trapezoidal intuitionistic fuzzy method for transferring the data into interval-valued trapezoidal multi-criteria for decision-making [34]. To efficiently handle the data, intuitionistic fuzzy sets(IFS) provide a triple vector to make appropriate decision making. Aribarg has introduced a modified fuzzy ant-miner (MFAM) that employs attributes and case weighting for training [35]. IFS was successfully applied for brain image segmentation for classifying tissues and tumors in presence of noise and artefacts [36, 37]. This motivated to use IFS for segmenting skin lesions in presence of artefacts.

Intuitionistic fuzzy set (IFS) theory for medical images has been proposed to handle images with a lot of uncertainties, as they are badly illumined with fuzzy. Direct segmentation of results often creates unusable results. In [38] Charia et al. used IFS theory to produce accurate diagnosing of diseases using cellular images. FCM clustering method has been proposed by Huang et al. [39] for image segmentation with rough set theory. The segmentation results of various clustering numbers using FCM where the image is distributed into various small regions based on the indistinguishable attributes and their relationship, have reduced error rates and improved segmentation of fuzzy boundary regions.

Advanced fuzzy set-theoretic techniques are very important and play a major role in the area of medical images. Image segmentation is performed on digital pathology images using the IFS method. This method results in strong results compared to other segmentation methods [40, 41]. Shaw et al. show that triangular intuitionistic fuzzy numbers with arithmetic procedures can be used to check the reliability of the fuzzy systems. To calculate imprecise failure, each component failure is taken into considerations by the triangular intuitionistic fuzzy numbers [42, 43].

Tilson et al. use FCM clustering programs for data analysis problems, and this method generate fuzzy classification for any set of given numerical data. The clustering method

used to group the subsets and generalized objective with least square method [44] is proposed.

Intuitionistic fuzzy c-means(IFCM) algorithm has been proposed for image segmentation in [45] for Brian images. Verma et al. use IFCM to handle the uncertainty. However, the results show that the method is very sensitive to noise and does not incorporate any local spatial information. From this, IIFCM (improved intuitionistic fuzzy c-means) has been proposed to handle the insensitive to noise and freedom of choosing the parameter when tuning is performed. IIFCM method results in significant performance increase compared to other existing methods [37, 46].

The clustering algorithms are based on IFS also suffer from initial centroid selection. In this paper, a novel algorithm is presented to obtain the melanoma regions from skin images. The proposed method identifies the initial regions using triangular fuzzy sets. The obtained regions are considered for different membership functions for IFS and the centroids are also initialized with mean values of the regions. The updating of the centroids and the membership functions of IFS are iterated until clusters are stable and exactly identify the melanoma regions.

The major contribution of the paper are:

- The paper has studied and analyzed triangular Intuitionistic Fuzzy Sets and its application to Skin cancer segmentation.
- Every fuzzy based clustering algorithm depends on initial centroid. In this paper, using the peaks and valleys of the histogram of the input image, the centroids are computed. The successive distance between valleys and peaks are considered for the parameters to define TMF.
- Applying TMF, the initial regions are computed that in turn are used to compute the initial centroids.
- TMF helps in identifying the initial clusters and regions and reduce the number of iterations needed for segmentation.
- TMF converges faster due to the initial centroids selection and the accuracy of the segmentation is increased.

The paper has different sections that explains the background in "Background", Triangular Intuitionistic Fuzzy C-Means (TIFCM) in "Proposed Methodology", implementation and experimental results analysis in "Implementation and Experimental Results" and finally conclusions and the future scope in "Conclusion".

Background

Challenges of Skin Cancer Detection

Skin cancer detection is a challenging task due to numerous artefacts associated with the skin medical images.

Irregular Shape, Size and Shade

Large changes in skin lesions have made accurate detection and segmentation of skin lesions difficult. Numerous factors, like lesion localization, its size, shape, skin hair, bubbles, blood vessels, uneven boundaries with fuzziness, and tone of the skin, need to be handled with preprocessing for accurate segmentation.

Image Acquisition Artefacts

The artefacts related to image acquisition include rule markers, imaging frames, low contrast, and illumination. Figure 1 depicts the artefacts that make skin cancer detection more complex.

Pre-processing and Post-processing

Preprocessing is performed on the data sets in different ways. The images are first converted to grayscale, and then resized because different data sets contain images of varying sizes.There is no additional pre-processing in this case because intuitionistic sets are used to obtain lesion belonging and non-belonging as well as fuzzy boundaries based on the membership function. Binarization is performed on the lesion-belonging region as part of the post-processing binarization to obtain the lesion region.

Fuzzy Sets and Triangular Fuzzy Membership Function

Definition 1 The definition of fuzzy set is notated by a membership function $\mu_{\tilde{a}}(e)$ where E is the universe of discourse. This function establishes a mapping between each element $e \in E$ to a real valued number in the range [0, 1]. This membership function reveals the grade of membership of the element e in $\mu_{\tilde{a}}(e)$. As the value of the function gets closer to unity, the higher will be the membership grade.

Definition 2 The function $\mu_{\tilde{a}}(e)$ for a triangular fuzzy number $\tilde{a} = (a1, a2, a3)$ is established as:

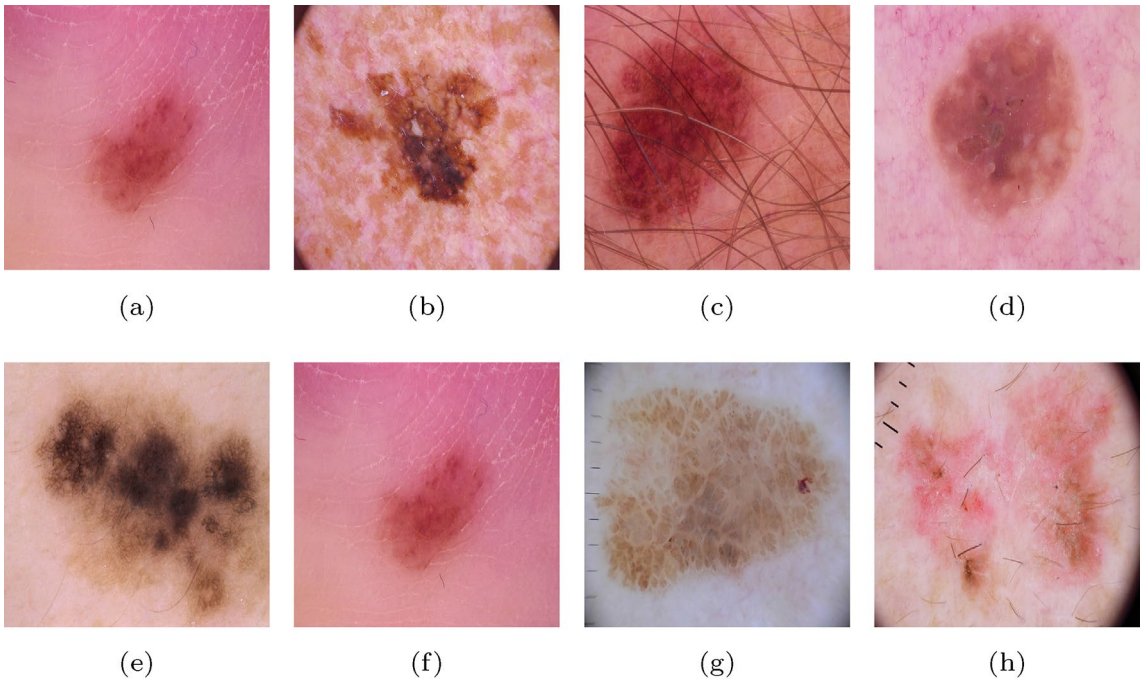

Fig. 1 Images from HAM10000 data set **a** skin tone, **b** irregular shape, **c** hair, **d** air bubble images, **e** fuzzy boundaries **f** cracked skin tones, **g** rule markers, **h** imaging frames

$$\mu_{\bar{a}}(e) = \begin{cases} 0 & \text{if } e < a1 \\ \frac{e-a1}{a2-a1} & \text{if } a1 < e \leq a2 \\ \frac{a3-e}{a3-a2} & \text{if } a2 < e < a3 \\ 0 & \text{Otherwise} \end{cases} \quad (1)$$

The values of the triplet ($a1$, $a2$, $a3$) are real numbers that confines to $a1 \leq a2 \leq a3$. The value of e at the triplet element $a2$ is the most likely value of the evaluation data and it is also observed as the supreme grade of $\mu_{\bar{a}}(e)$. On the other hand, the minimum grade of e at $\mu_{\bar{a}}(e)$ is the least likely value to be evaluated from the membership function i.e., $\mu_{\bar{a}}(e) = 0$. The range of evaluation data is bounded between the constants [$a1$, $a3$], which is an implication of degree of fuzziness of the evaluation data.

Intuitionistic Fuzzy Sets

Generalization of fuzzy sets is characterised by membership, non-membership and hesitancy values [47]. The degree of belongingness to a cluster determines the membership and non-membership property of the elements. The dilemma of a particular pixel belonging to a specific cluster is determined by the hesitancy. Hesitancy adds precision to the imperfect knowledge obtained from the fuzzy sets.

$$A = \{(e, \mu_A(e), \pi_A(e)) \mid e \in E\} \quad (2)$$

with $\gamma_A(e) = 1 - (\mu_A(e) + \pi_A(e))$ where the functions $\mu_A(e), \pi_A(e)$ indicate the degree to which an element belongs or does not belong to the finite set E. The intuitionistic fuzzy index is determined by $\gamma_A(e)$ signifies the degree of hesitation of an element. The necessary conditions to be satisfied by an element $e \in E$ that is defined as IFS is given by $0 \leq \mu_A(e), \gamma_A(e), \pi_A(e) \leq 1$. The bias, noise and assignment of an element to a particular cluster is precisely represented by the three functions.

Data Sets

Different data sets available to work with skin cancer algorithms are explained below and are presented in Table 1.

PH2 [48] consists of epiluminoscopy images,also known as dermoscopic images having the size of 765X574 pixel values. There are 200 images in this dataset of melanocytic

Table 1 Data sets used for simulation

Dimension	Dataset	Number of images	Image size
2D	PH2	200	765×574
2D	ISIC 2019	25331	varying × varying
2D	HAM10000	10015	600×450

lesions, including nevi, sensitive nevi, and melanomas.This dataset also contains numerous image descriptors.

ISIC 2019 dataset is categorized into 8 different classes of dermoscopic images for training and testing. The datasets are available with and without metadata and contain a total of 25,331 images. Groundtruths are also available for testing on standard images of lesions.This dataset is derived from the BCN20000, HAM10000, and MSK datasets [46, 49].

HAM10000 [50] as the name indicates, it contains 10,015 images for training that were classified in to different dermatoscopic images in the realm of pigmented lesions collected from varied populations. They were collected, confirmed and stored through different modalities rate [50]. They are available for the research and public use in the ISIC collection.

Proposed Methodology

This section mainly concentrates on the flow of segmentation performed on skin images using triangular intuitionistic fuzzy sets.

Triangular Membership Based Fuzzy Region Determination

The fuzzy functions highly impact the segmentation performance as these are necessary for producing clusters. The proposed method presents a novel approach by identifying the initial regions with the triangular membership functions, which act as the input to the intuitionistic fuzzy

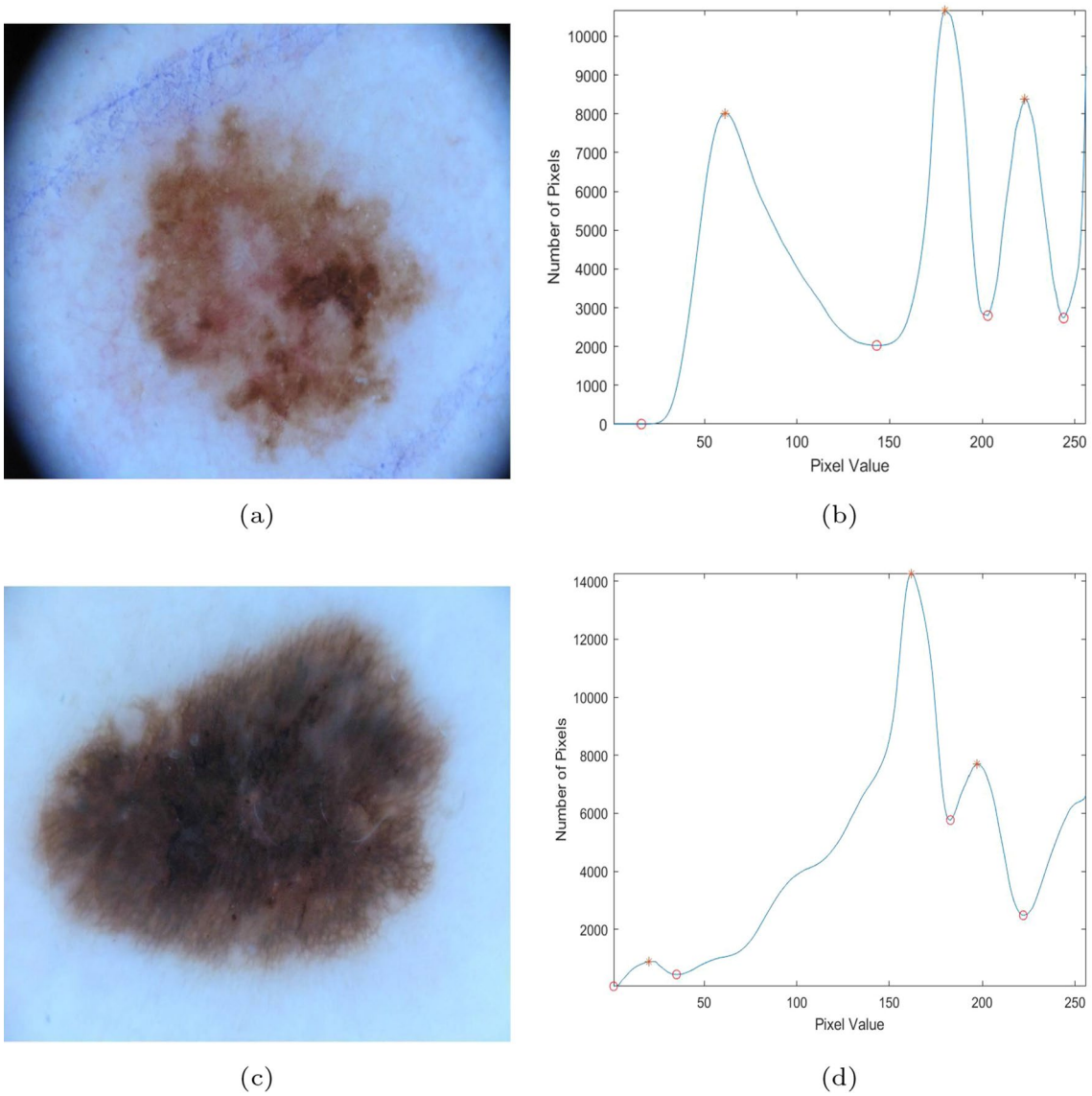

Fig. 2 **a**, **c** ISIC sample images, **b**, **d** valleys and peaks of the images

C-means. The observed image having the size $m \times n$ is denoted as $E = \{e_i / e_i$ represents ith pixel value in the image $\}$. To apply triangular membership function a, b and c values are needed. These values are calculated from the gray values associated with the peaks and valleys of the histogram of the image [51]. Figure 2 show the ISIC images and their corresponding peaks and valleys. Every sequence of valley, peak and valley will be treated as $a1$, $a2$ and $a3$ that will extract the membership $\mu_{\tilde{a}}(e)$ for the regions using Eq. 1.

The regions obtained from the triangular membership function are given as input to the intuitionistic fuzzy c-means. Figure 3 shows the regions extracted using triangular membership function.

Triangular Intuitionistic Fuzzy c-Means (TIFCM)

The regions obtained from the triangular membership function are used to find the centroids needed to perform intuitionistic fuzzy c-means. Many image segmentation works based on IFS are proposed in [37, 52, 53]. The image E is correlated to intuitionistic fuzzy with the below equation

$$A = \{(e_i, \mu(e_i), \pi(e_i)) \mid e_i \in E\} \tag{3}$$

To find $\mu(e_i), \pi(e_i)$ and $\gamma(e_i)$, membership functions, the three regions obtained with a, b, c of triangular membership function is considered as deterministic region $D(e_i)$,$H(e_i)$ and other region as indeterminacy region $I(e_i)$. Compute the mean value of every region to obtain the initial centroids C_j where $1 < j < n$(n is the 3 for three regions).

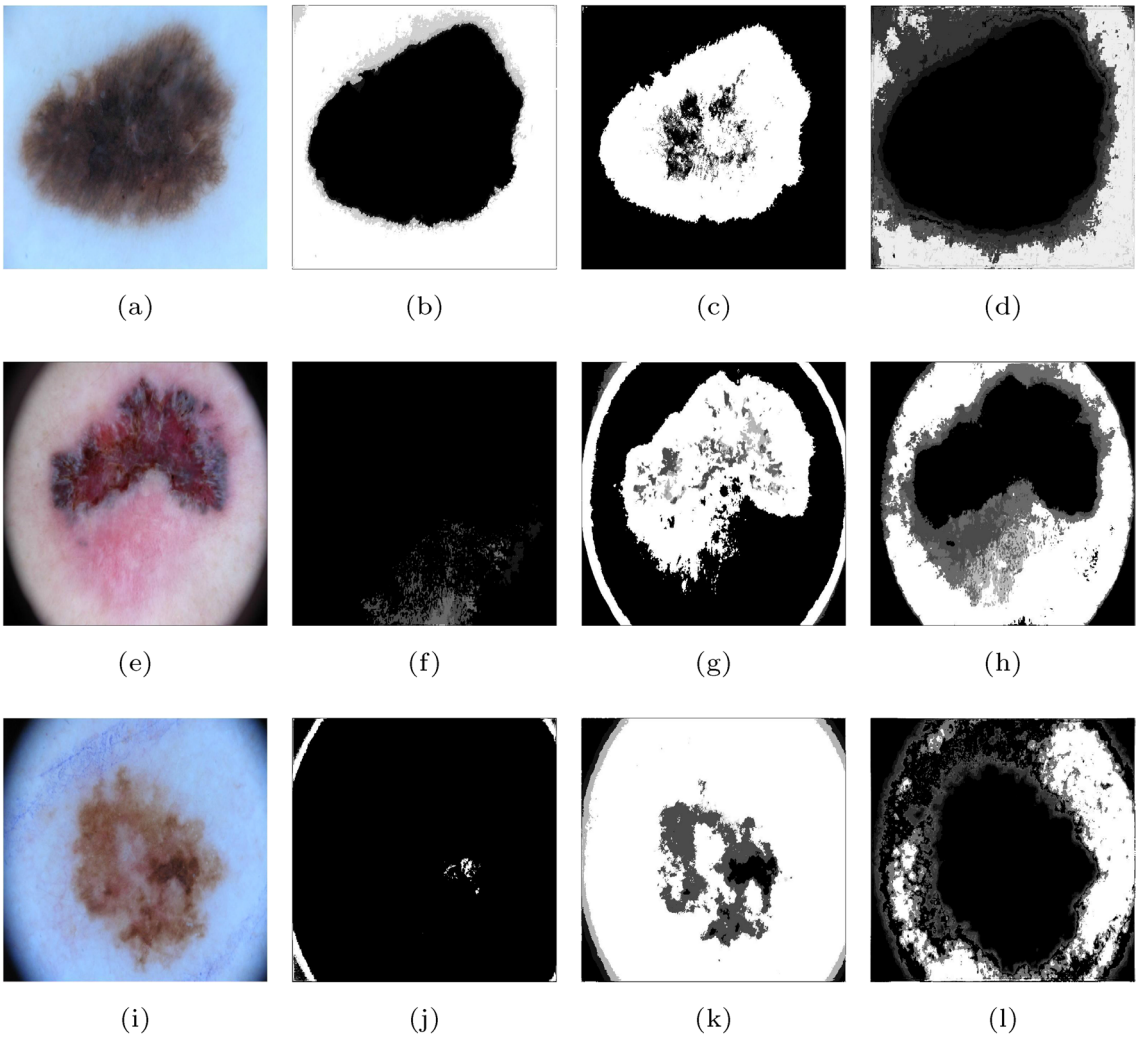

Fig. 3 **a**, **e**, **i** Images from ISIC data set, **b**, **f**, **j** regions extracted for values $a1 < e_i \leq a2$, **c**, **g**, **k** regions extracted for values $a2 < e_i \leq a3$, **d**, **h**, **l** other region for values $e_i \leq a1$ and $e_i \geq a3$

The computation of membership value $\mu(e_i)$ is performed with the deterministic region $D(e_i)$ and the centroids with the below Eq. 4.

$$\mu(e_i) = \frac{1}{\sum_{j=1}^{n} \left(\frac{||D(e_i)-C_j||}{\sum_{n,c!=j}^{c=1} ||D(e_i)-C_c||} \right)^{\frac{2}{m-1}}} \tag{4}$$

where C_j is the centroid of jth cluster (here, mean value of $(D(e_i))$ and C_c is the centroid values of regions other than jth cluster (here, $H(e_i), I(e_i)$) are obtained from triangular membership function). Compute $\pi(e_i)$, and $\gamma(e_i)$ with the help of $I(e_i)$ and $H(e_i)$ by making use of Eqs.(5)-(6).

$$\pi(e_i) = \frac{1}{\sum_{j=1}^{n} \left(\frac{||I(e_i)-C_j||}{\sum_{n,c!=j}^{c=1} ||I(e_i)-C_c||} \right)^{\frac{2}{m-1}}} \tag{5}$$

$$\gamma(e_i) = \frac{1}{\sum_{j=1}^{n} \left(\frac{||H(e_i)-C_j||}{\sum_{n,c!=j}^{c=1} ||H(e_i)-C_c||} \right)^{\frac{2}{m-1}}} \tag{6}$$

The IFS partition matrix $\mu_{IFS}(e_i)$ and cluster centroid $C(\mu(e_i))$ are updated using the below equations.

$$\mu_{IFS}(e_i) = \mu(e_i) + \pi(e_i) + \gamma(e_i) \tag{7}$$

$$C(\mu(e_i)) = \frac{\sum_{e_i \in E} (\mu(e_i))^m (e_i)}{\sum_{e_i \in E} (\mu(e_i))^m} \tag{8}$$

Find the other centroids using the Eq. 8 for $\pi(e_i)$ and $\gamma(e_i)$. Here, m indicates the fuzzification constant given by user. The membership function converts to be crisp and binary if the values m nears to 1 otherwise fuzzy and blurred with increased value [54]. Good segmentation results are produced for vast data with $1.5 < m < 3$ and generally 2 is considered[55, 56].

Triangular intuitionistic fuzzy c-means is also iterative similar to other clustering algorithms. It finds the three regions using Eqs. 4, 5, 6 and obtains the new centroids using Eq. 8 repeatedly and stops when the clusters are stable. The stability of cluster is computed with the similarity coefficient based on the Hamming distance between the previous clusters $\mu(e_i))^l, \pi(e_i)^l$ and $\gamma(e_i)^l$ and present cluster $\mu(e_i))^{l+1}, \pi(e_i)^{l+1}$ and $\gamma(e_i)^{l+1}$. The hamming distance is given with the equation

$$\begin{aligned} sc = \sum_{i=1}^{M*N} & \mid \mu_(e_i)^l - \mu_(e_i)^{l+1} \mid \\ & + \mid \pi(e_i)^l - \pi(e_i)^{l+1} \mid \\ & + \mid \gamma(e_i)^l - \gamma(e_i)^{l+1} \mid \end{aligned} \tag{9}$$

Triangular Intuitionistic Fuzzy c-Means Clustering Algorithm (TIFCM)

The step-wise algorithm of Triangular intuitionistic fuzzy is listed below.

Algorithm 1 Segmentation algorithm for images with generalized triangular intuitionistic fuzzy sets

INPUT: TIFCM image E and ϵ exit criteria with 0.01.

OUTPUT: n number of clusters to be generated for representing the regions of skin image contain a, b, c values for each regions using method defined by [51]

1 Obtain a,b,c values for each regions using method defined by [51].
2 Obtain the three regions $D(e_i)$,$H(e_i)$ and $I(e_i)$ as per Eq. 1 .
3 Find the cluster centroids C_j from the regions by finding the mean value of the region.
4 while true
4.1 for every j in n clusters and every e_i in E obtain three intuitionistic membership function values using Eq. 4-6
4.2 Update the partition matrix $\mu_{IFS}(e_i)$ and the cluster centroid C_j using Eq. 7 and Eq. 8.
4.3 Estimate the similarity coefficient(sc) using Eq.9
4.4 If $sc \leq \epsilon$ then break else compute $\mu_{IFS}(e_i)^l = \mu_{IFS}(e_i)^{l+1}$ and repeat 4.
5 with stable $\mu_(e_i)$, $\gamma_(e_i)$ and $\pi_(e_i)$ obtain n clusters.

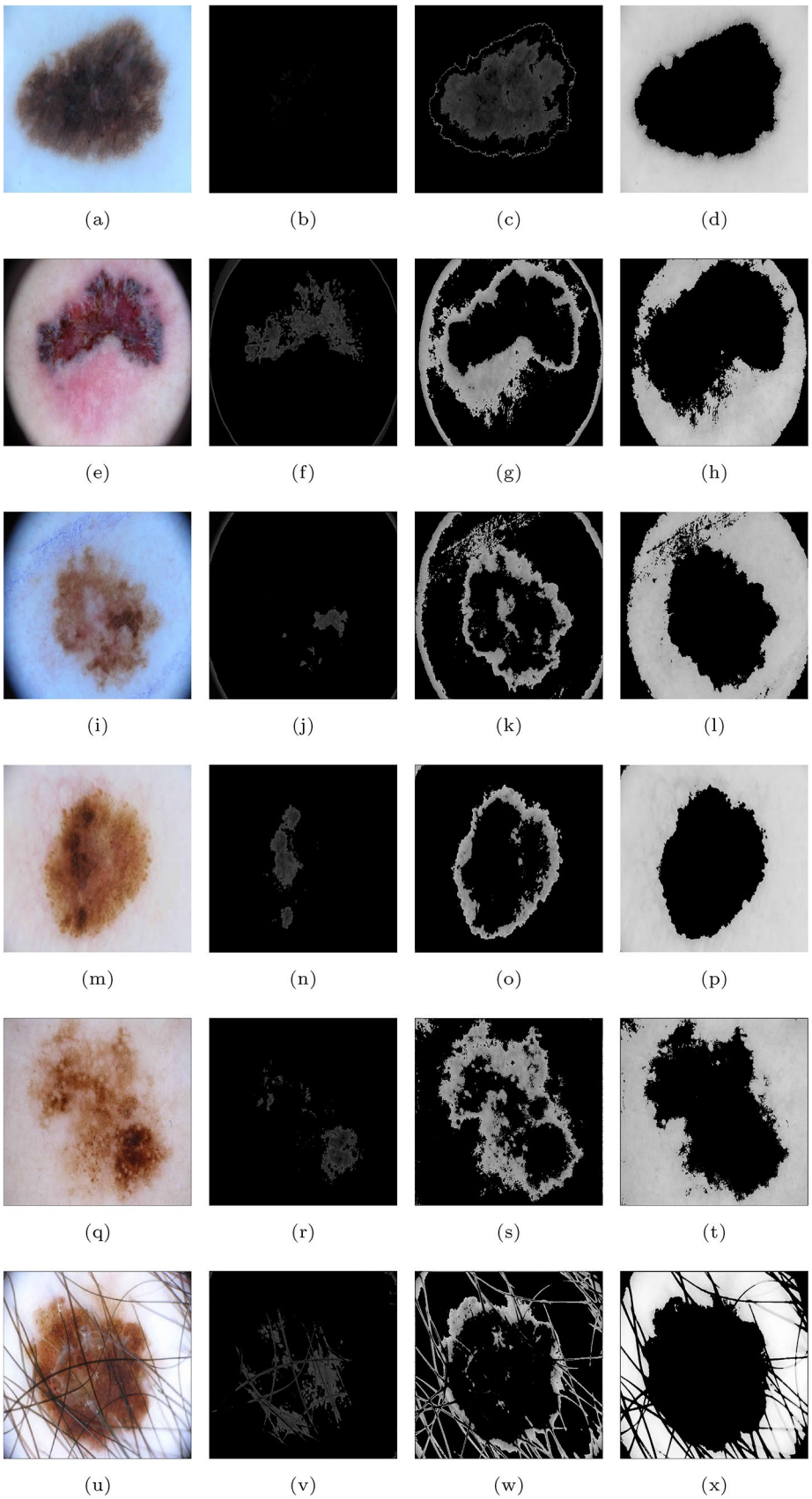

Fig. 4 Segmentation results of proposed algorithm TIFCM for different images of ISIC data set. (Column 1) Original images of ISIC data sets, (Column 2) Deterministic region depicting cancer region, (Column 3) Indeterminacy regions (Column 4) Hesitance regions

Implementation and Experimental Results

Experimental Setup

To find the efficacy of the proposed algorithm TIFCMM, The ISIC 2016, HAM10000 2019 data set [49] and PH2 [48] data set is used. The data set contains the skin images with diagnostic, clinical, technical and database attributes based images. The proposed TIFCM algorithm is worked out with MATLAB software on i5 processor. The total number of clusters n is assigned as 3 in the proposed algorithm to determine the three regions. The centroid values are initialised through the triangular membership functions. The difference between the subsequent clusters is fixed as the exit criteria, which is 0.01.

As part of pre-processing the images are resized to 512×640 as the image sizes vary for ISIC, PH2, HAM10000 data sets. In post processing of the proposed algorithm, the deterministic final region is converted to black and white to compare with the ground truths.

The segmentation results of the TIFCM algorithm on various skin images is shown in Fig. 4. Column 1shows the Original images of ISIC data sets. The images (a) ISIC_0000000,(e) ISIC_0000008 (i)ISIC_0000049 (m) ISIC_0000008 (q) ISIC_0000002 (u) ISIC_0000043 are shown in Column 1 and are used to extract malignant region using proposed TIFCM. Column 2 shows the Deterministic region depicting cancer region, Column 3 depicting Indeterminacy regions and Column 4 showing the Hesitance regions extracted from the stable clusters of TIFCM. Further, in Fig. 5 the segmentation results of images ISIC0034329, ISIC0034332, ISCI0034337 and ISIC0034343 of ISIC 2019 data set are presented. The subjective analysis show that the lesion was extracted efficiently using the proposed method.

Figure 6 exhibits the results of TIFCM algorithm for different images like malignant melanoma, melanoma, benign melanoma, common nevus, a typical nevus image that are commonly identified skin diseases of PH2 data set. The lesion detection of these images are compared with their ground truths [7]. The results showed that the proposed algorithm performs very well when compared to other algorithms. The comparative analysis of the proposed algorithms with other state of art techniques namely KM [57], FCM [55], RFCM [58], and GRIFCM [37] is given in Fig 7. The detailed analysis with other segmentation algorithms reveals that the proposed algorithm gives improved cancer region segmentation.

Quantitative Analysis

The segmentation results are analysed quantitatively using the performance measures namely, segmentation accuracy (SA), Jaccard's coefficient (JC) and Dice coefficient (DC).

$$\text{Jaccard coefficient} = \frac{E1 \bigcap E2}{E1 \bigcup E2} \tag{10}$$

$$\text{Dice coefficient} = \frac{2 \mid E1 \bigcap E2 \mid}{\mid E1 \mid + \mid E2 \mid} \tag{11}$$

where $E1$ is the ground truth image. $E2$ is the resultant segmented image,

$$\text{Segmentation Accuracy} = \frac{TP + FN}{TP + FN + TN + FN} \tag{12}$$

where,

1. True positive (TP): Ratio of sum of true pixels in the E2 detected in E1.
2. True negative (TN): Ratio of sum of true pixels in the E2 falsely segmented as negative in E1.
3. False positive (FP): Ratio of sum of false pixels in E2 falsely segmented as positive in E1.
4. False negative (FN): Ratio of sum of false pixels in E2 detected as negative in E1.

The SA, JC, DC, precision, specificity and sensitivity measures are given in Table 2. These performance measures are calculated for different skin disease, namely, malignant melanoma, melanoma, benign melanoma, common nevus, typical nevus images of ISIC data set images. The results proved that the proposed algorithms have efficiently extracted the lesion of an cancerous tissues. The average JC value of 0.85, SA of 0.90 is achieved for with the proposed TIFCM. The quality of segmentation can be assessed by observing the segmentation JC value with 0.8 or above indicating the visual "correctness". It is observed that for 100 images from ISIC 2019 the observant agreement for JC value is considered as 0.786[49]. It is observed that, the fall in JC value below 0.7, the "correctness" of the segmentation can be debated. With the proposed method,78 out of 100 images fell above JC of 0.7, 10 images fell at or below 0.7, rest images fell below 0.6.

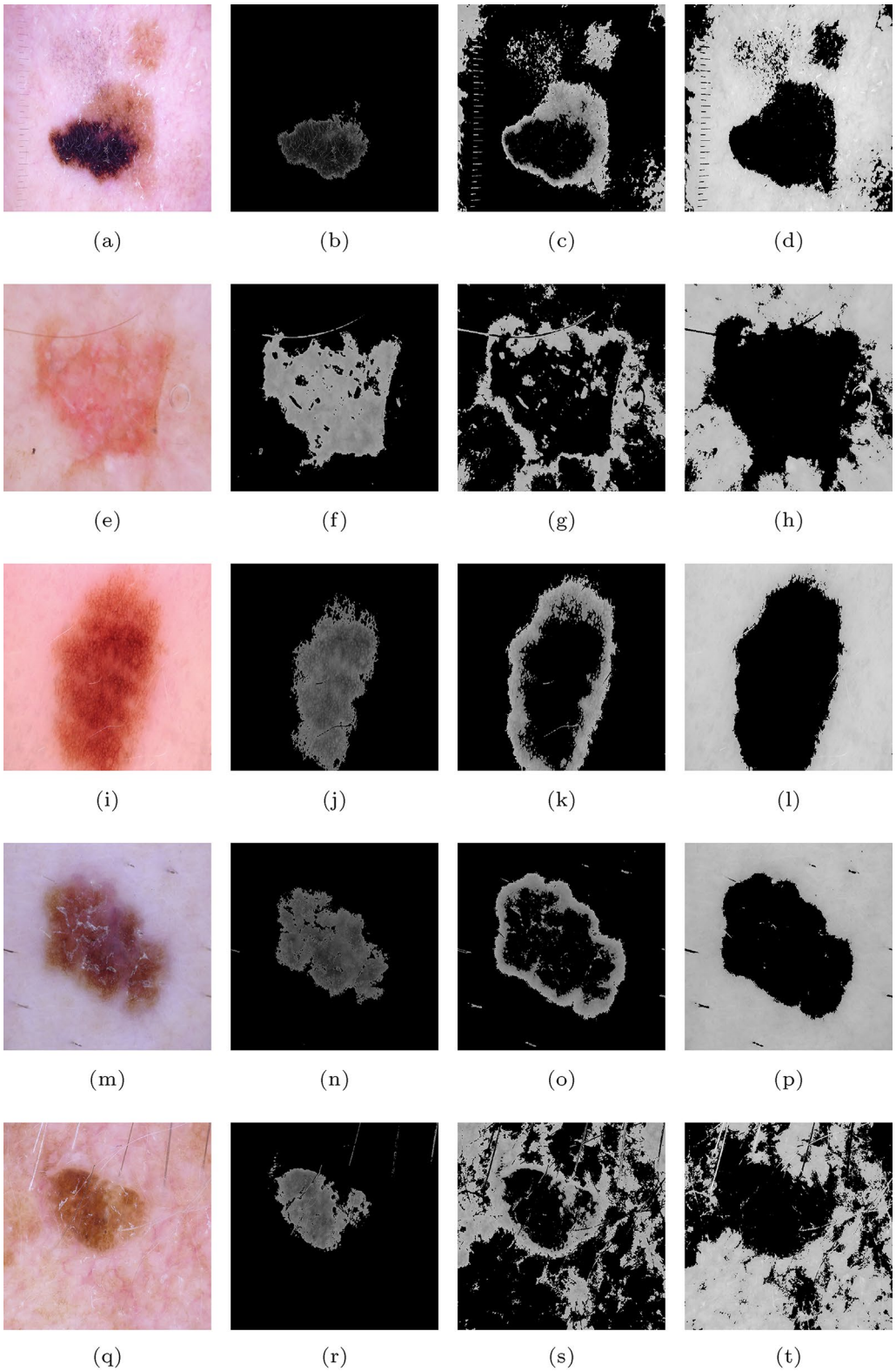

Fig. 5 Segmentation results of proposed algorithm `TIFCM` for ISIC_0034329, ISIC_0034332, ISCI_0034337 and ISIC_0034343 of ISIC 2019 data set. (Column 1) Original images of ISIC data sets, (Column 2) Deterministic region depicting cancer region, (Column 3) Indeterminacy regions (Column 4) Hesitance regions

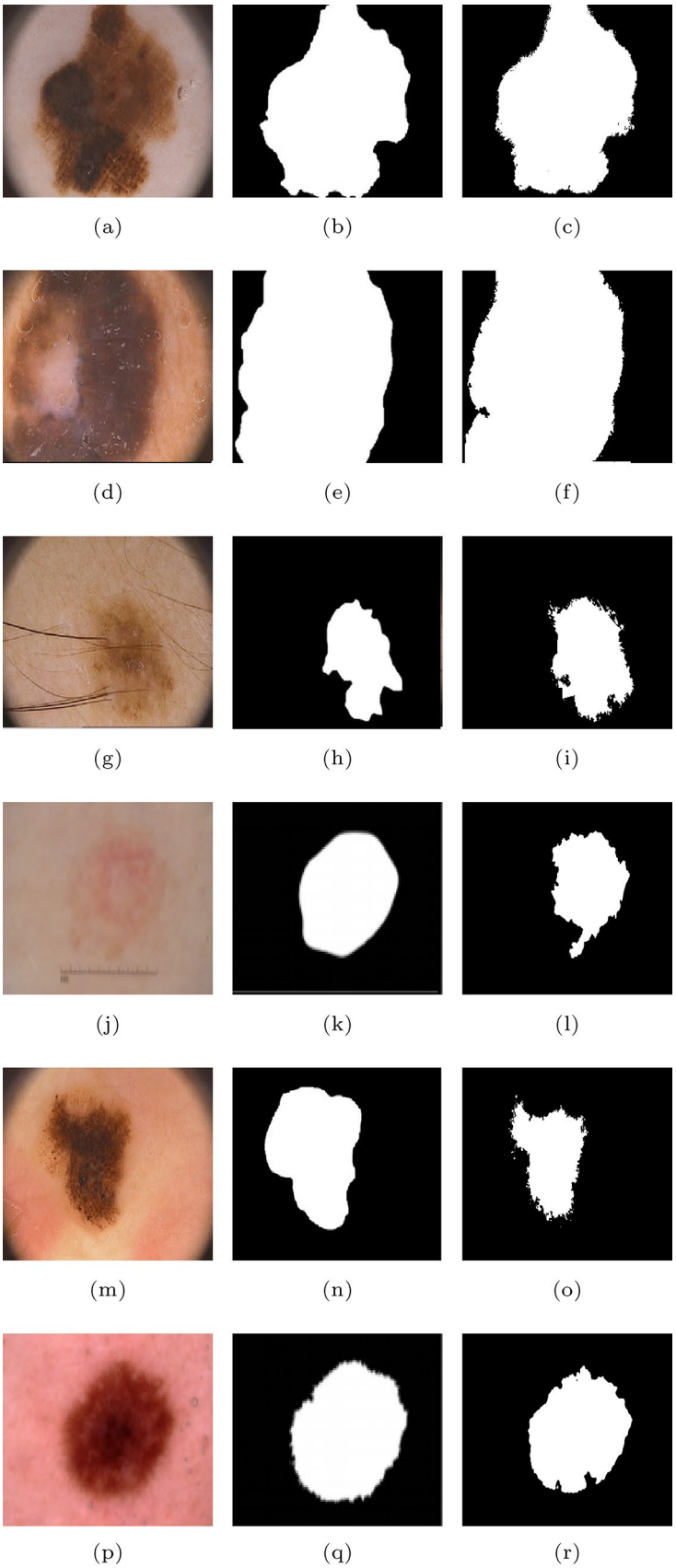

Fig. 6 Lesion segmentation of different PH2 data set images. (Row 1) **a** Malignant melanomas image IMD063, **b** Ground Truth(GT), **c** extracted using TIFCM. (Row 2) **d** Melanoma image IMD058, **e** GT of IMD058, **f** extracted using TIFCM. (Row 3) **g** A typical Nevus image IMD048, **h** GT of IMD048, (i)extracted using TIFCM. (Row 4) **j** Common Nevus image ISIC_0012253, **k** GT of (**j**), **l** extracted using TIFCM.(row 5) **m** Benign melanoma image IMD075, **n** GT of IMD075, **o** extracted using TIFCM. (row 6) **p** Benign melanoma image ISIC_0000125, **q** GT of **p**, **r** extracted using TIFCM

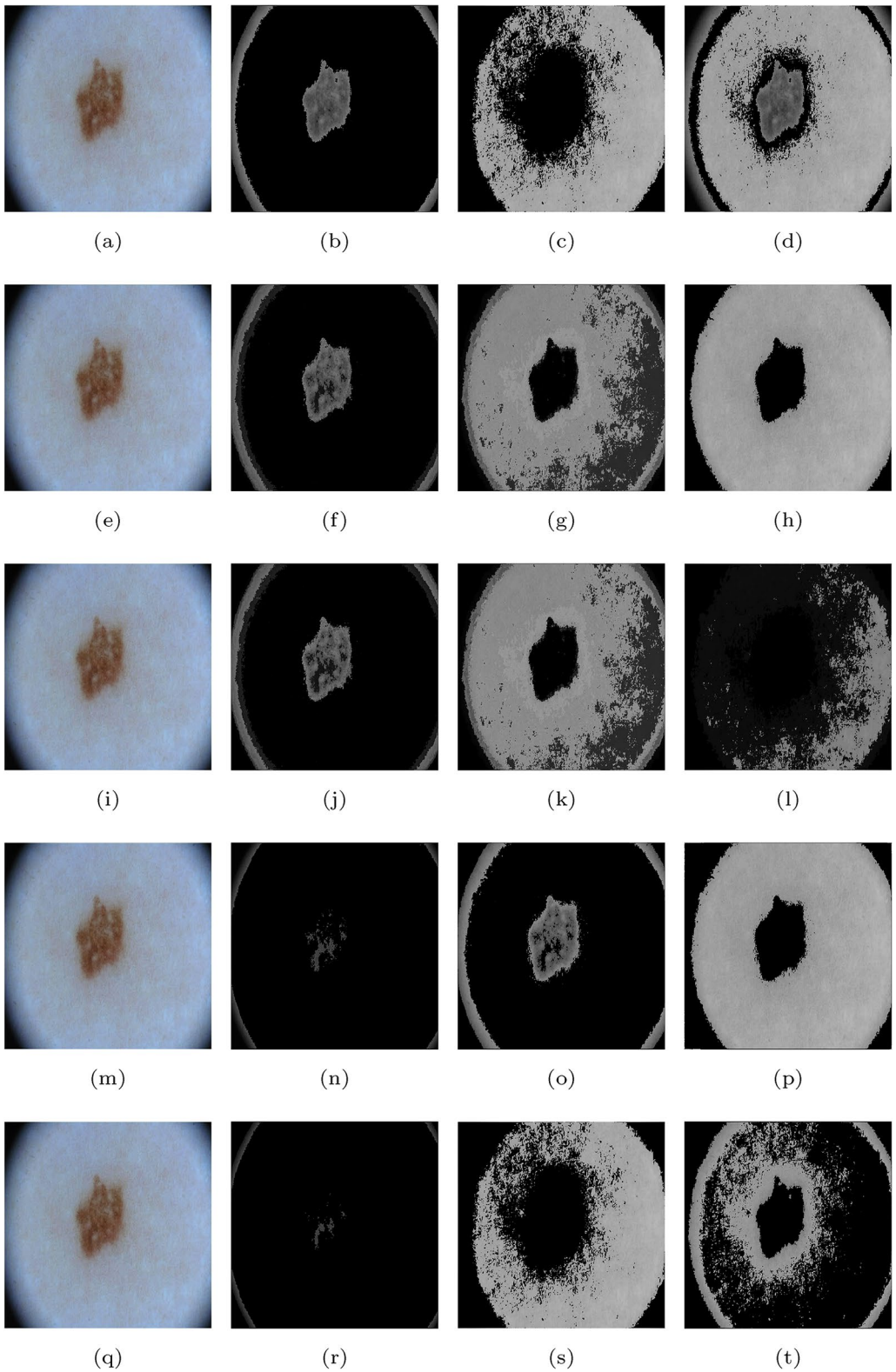

Fig. 7 Comparison of Algorithms applied to ISIC_0000006 for Benign nevus detection (Row 1) Segmentation with KM, (Row 2) Segmentation with FCM, (Row 3) Segmentation with RFCM, (Row 4) Segmentation with GRIFCM, (Row 5) Segmentation with TIFCM

Table 2 Comparisons of performance measures for the images in Fig. 3

Images	SA	JC	DC	Precision	Sensitivity	Specificity
Malignant melanoma	0.9059	0.8799	0.8438	0.8797	0.9206	0.8935
Melanoma	0.9308	0.9341	0.7939	0.9396	0.9530	0.8915
A typical nevus	0.9185	0.7424	0.8071	0.7468	0.7868	0.9585
Common nevus	0.8719	0.8323	0.8123	0.8623	0.9880	0.8639
Benign melanoma	0.8689	0.7921	0.8528	0.8121	0.9853	0.8520

Table 3 Comparisons of performance measures for different segmentation algorithms

Algorithm	SA	JC	Sensitivity	Specificity	DC
Yolo et al. [30]	0.929	0.795	0.836	0.940	0.881
Yuan et al. [8]	0.930	0.765	0.825	0.975	0.849
Li et al. [32]	0.932	0.7620	0.820	0.978	0.847
Lin et al. [33]	–	0.620	–	–	0.770
FCM [59]	0.884	0.665	0.869	0.923	0.884
TIFCM	0.905	0.856	0.952	0.862	0.830

Table 4 Execution time comparison for different algorithms

KM	FCM	RFCM	GRIFCM	TIFCM
38.5 ± 2.3	35.8 ± 2.5	32.4 ± 2.1	20.5 ± 3.2	16.56 ± 2.5

To depict the efficiency and robustness of the proposed TIFCM method, a comparison with the latest methods in the literature, are shown in Table 3. The methods used in the comparison are executed on ISIC 2017 challenge and are ranked based on the Jaccard's coefficient. It is clear from the table that the JC values produced with the proposed method has an marginal increment over other lesion segmentation algorithms.Also, the improved sensitivity values are observed with the proposed method. In contrast, the deep learning methods have exhibited high segmentation accuracy and specificity. The proposed method dice coefficients are inline with the results of the deep learning methods (Table 3). In Table 4 the execution times of proposed method in comparision to the existing algorithms are presented. The proposed TIFCM method shows improved performace as the initial centroids are chosen with the histrogram peaks and valleys.

The efficacy of the proposed method is also compared with the method FCM classification of pixels with histogram thresholds [59]. The SA, JC and sensitivity values are significantly improved with the proposed methods while the specificity and DC values are less with the proposed method.

Conclusion

Computer-aided detection of malignant melanoma skin cancer with the use of skin images has tremendously assisted clinicians. Skin cancer detection has become more difficult due to a variety of factors such as artefacts in skin images, non-homogeneous intensities, and low contrast images.In this paper, we present a novel `TIFCM` algorithm for skin image segmentation. The triangular membership function is used to extract the initial regions and centroids. This avoids the initial selection of centroids, which is the drawback of every clustering algorithm. The triangular membership based centroids and regions assist in the faster stability of clusters, reducing the execution time. The regions extracted are used as initial inputs to calculate the membership functions of the intuitionistic fuzzy c-means that effectively handle the uncertainty in the skin images.

Funding Not applicable.

Data availability The data will be made available on request from the author.

Declarations

Conflict of interest The authors declare that there is no conflict of interest.

References

1. Santosh K, Wendling L, Antani S, Thoma GR. Overlaid arrow detection for labeling regions of interest in biomedical images. IEEE Intell Syst. 2016;31(3):66–75.
2. Santosh K, Roy PP. Arrow detection in biomedical images using sequential classifier. Int J Mach Learn Cybern. 2018;9(6):993–1006.
3. Oliveira RB, Mercedes Filho E, Ma Z, Papa JP, Pereira AS, Tavares JMR. Computational methods for the image segmentation of pigmented skin lesions: a review. Comput Methods Prog Biomed. 2016;131:127–41.
4. Koundal D, Sharma B. Advanced neutrosophic set-based ultrasound image analysis. In: Neutrosophic Set in Medical Image Analysis, 2019; 51–73. Elsevier.

5. Al-Masni MA, Al-Antari MA, Choi M-T, Han S-M, Kim T-S. Skin lesion segmentation in dermoscopy images via deep full resolution convolutional networks. Comput Methods Prog Biomed. 2018;162:221–31.
6. Olugbara OO, Taiwo TB, Heukelman D. Segmentation of melanoma skin lesion using perceptual color difference saliency with morphological analysis. Math Prob Eng 2018;2018.
7. Pennisi A, Bloisi DD, Nardi D, Giampetruzzi AR, Mondino C, Facchiano A. Skin lesion image segmentation using delaunay triangulation for melanoma detection. Comput Med Imaging Graph. 2016;52:89–103.
8. Yuan Y. Automatic skin lesion segmentation with fully convolutional-deconvolutional networks. 2017. arXiv preprint arXiv:1703.05165.
9. Korotkov K, Garcia R. Computerized analysis of pigmented skin lesions: a review. Artif Intell Med. 2012;56(2):69–90.
10. Otsu N. A threshold selection method from gray-level histograms. IEEE Trans Syst Man Cybern. 1979;9(1):62–6.
11. Yüksel ME, Borlu M. Accurate segmentation of dermoscopic images by image thresholding based on type-2 fuzzy logic. IEEE Trans Fuzzy Syst. 2009;17(4):976–82.
12. Barata C, Ruela M, Francisco M, Mendonça T, Marques JS. Two systems for the detection of melanomas in dermoscopy images using texture and color features. IEEE Syst J. 2013;8(3):965–79.
13. Zhou H, Schaefer G, Sadka AH, Celebi ME. Anisotropic mean shift based fuzzy c-means segmentation of dermoscopy images. IEEE J Select Top Signal Process. 2009;3(1):26–34.
14. Castillejos H, Ponomaryov V, Nino-de-Rivera L, Golikov V. Wavelet transform fuzzy algorithms for dermoscopic image segmentation. Computat Math Methods Med 2012;2012.
15. Castiello G, Castellano G, Fanelli AM. Neuro-fuzzy analysis of dermatological images. In: 2004 IEEE International Joint Conference on Neural Networks (IEEE Cat. No. 04CH37541), 2004;4:3247–3252. IEEE
16. Maeda J, Kawano A, Yamauchi S, Suzuki Y, Marçal A, Mendonça T. Perceptual image segmentation using fuzzy-based hierarchical algorithm and its application to dermoscopy images. In: 2008 IEEE Conference on Soft Computing in Industrial Applications, 2008;66–71. IEEE
17. Arroyo JLG, Garcia-Zapirain B. Segmentation of skin lesions based on fuzzy classification of pixels and histogram thresholding. CoRR .2017. arXiv:1703.03888
18. Ma L, Staunton RC. Analysis of the contour structural irregularity of skin lesions using wavelet decomposition. Pattern Recogn. 2013;46(1):98–106.
19. Celebi ME, Iyatomi H, Schaefer G, Stoecker WV. Lesion border detection in dermoscopy images. Comput Med Imaging Graph. 2009;33(2):148–53.
20. Erkol B, Moss RH, Joe Stanley R, Stoecker WV, Hvatum E. Automatic lesion boundary detection in dermoscopy images using gradient vector flow snakes. Skin Res Technol. 2005;11(1):17–26.
21. Riaz F, Naeem S, Nawaz R, Coimbra M. Active contours based segmentation and lesion periphery analysis for characterization of skin lesions in dermoscopy images. IEEE J Biomed Health Inform. 2018;23(2):489–500.
22. Rajinikanth V, Madhavaraja N, Satapathy SC, Fernandes SL. Otsu's multi-thresholding and active contour snake model to segment dermoscopy images. J Med Imaging Health Inform. 2017;7(8):1837–40.
23. Vasconcelos FFX, Medeiros AG, Peixoto SA, Rebouças Filho PP. Automatic skin lesions segmentation based on a new morphological approach via geodesic active contour. Cogn Syst Res 2019;55,44–59.
24. Mondal B, Das N, Santosh K, Nasipuri M. Improved skin disease classification using generative adversarial network. In: 2020 IEEE 33rd International Symposium on Computer-Based Medical Systems (CBMS), 2020;pp. 520–525. IEEE
25. Maiti A, Chatterjee B, Santosh K. Skin cancer classification through quantized color features and generative adversarial network. Int J Ambient Comput Intell (IJACI). 2021;12(3):75–97.
26. Brinker TJ, Hekler A, Utikal JS, Grabe N, Schadendorf D, Klode J, Berking C, Steeb T, Enk AH, von Kalle C. Skin cancer classification using convolutional neural networks: systematic review. J Med Internet Res. 2018;20(10):11936.
27. Sultana NN, Puhan NB. Recent deep learning methods for melanoma detection: a review. In: International Conference on Mathematics and Computing, 2018;pp. 118–132. Springer
28. Marka A, Carter JB, Toto E, Hassanpour S. Automated detection of nonmelanoma skin cancer using digital images: a systematic review. BMC Med Imaging. 2019;19(1):21.
29. Munir K, Elahi H, Ayub A, Frezza F, Rizzi A. Cancer diagnosis using deep learning: a bibliographic review. Cancers. 2019;11(9):1235.
30. Ünver HM, Ayan E. Skin lesion segmentation in dermoscopic images with combination of yolo and grabcut algorithm. Diagnostics. 2019;9(3):72.
31. Ghosh S, Bandyopadhyay A, Sahay S, Ghosh R, Kundu I, Santosh K. Colorectal histology tumor detection using ensemble deep neural network. Eng Appl Arti Intell. 2021;100:104202.
32. Li Y, Shen L. Skin lesion analysis towards melanoma detection using deep learning network. Sensors. 2018;18(2):556.
33. Lin BS, Michael K, Kalra S, Tizhoosh HR. Skin lesion segmentation: U-nets versus clustering. In: 2017 IEEE Symposium Series on Computational Intelligence (SSCI), 2017;7. IEEE
34. Ban AI, Tuse DA. Trapezoidal/triangular intuitionistic fuzzy numbers versus interval-valued trapezoidal/triangular fuzzy numbers and applications to multicriteria decision making methods. Notes Intuit Fuzzy Sets. 2014;20(2):43–51.
35. Aribarg T, Supratid S, Lursinsap C. Optimizing the modified fuzzy ant-miner for efficient medical diagnosis. Appl Intell. 2012;37(3):357–76. https://doi.org/10.1007/s10489-011-0332-x.
36. Dubey YK, Mushrif MM, Mitra K. Segmentation of brain mr images using rough set based intuitionistic fuzzy clustering. Biocybernet Biomed Eng. 2016;36(2):413–26.
37. Namburu A, Samayamantula SK, Edara SR. Generalised rough intuitionistic fuzzy c-means for magnetic resonance brain image segmentation. IET Image Process. 2017;11(9):777–85.
38. Chaira T. A rank ordered filter for medical image edge enhancement and detection using intuitionistic fuzzy set. Appl Soft Comput J. 2012;12(4):1259–66. https://doi.org/10.1016/j.asoc.2011.12.011.
39. Huang H, Meng F, Zhou S, Jiang F, Manogaran G. Brain image segmentation based on fcm clustering algorithm and rough set. IEEE Access. 2019;7:12386–96. https://doi.org/10.1109/ACCESS.2019.2893063.
40. Uma Rani R, Amsini P. Triangular intuitionistic fuzzy set for nuclei segmentation in digital cancer pathology. IOSR J Eng. 2018.
41. Mondal SP, Goswami A, De Kumar S. Nonlinear triangular intuitionistic fuzzy number and its application in linear integral equation. Adv Fuzzy Syst. 2019;2019:1–14. https://doi.org/10.1155/2019/4142382.
42. Shaw AK, Roy TK. Trapezoidal intuitionistic fuzzy number with some arithmetic operations and its application on reliability evaluation. Int J Math Oper Res. 2012;5(1):55. https://doi.org/10.1504/ijmor.2013.050512.
43. Li DF. A ratio ranking method of triangular intuitionistic fuzzy numbers and its application to MADM problems. Comput Math Appl. 2010;60(6):1557–70.
44. Tilson L.V, Excell P.S, Green R.J. A generalisation of the fuzzy c-means clustering algorithm. In: International Geoscience and

Remote Sensing Symposium, 'Remote Sensing: Moving Toward the 21st Century'., 1988;3:1783–1784. https://doi.org/10.1109/IGARSS.1988.569600
45. Verma H, Agrawal R.K, Sharan A. An improved intuitionistic fuzzy c-means clustering algorithm incorporating local information for brain image segmentation. Appl. Soft Comput. J. 2016;46. https://doi.org/10.1016/j.asoc.2015.12.022
46. Codella N.C.F, Gutman D, Celebi M.E, Helba B, Marchetti M.a, Dusza S.W, Kalloo A, Liopyris K, Mishra N, Kittler H, Halpern A. Skin lesion analysis toward melanoma detection: a challenge at the 2017 International symposium on biomedical imaging (ISBI), hosted by the international skin imaging collaboration (ISIC). Proceedings - International Symposium on Biomedical Imaging 2018-April, 2018;168–172. https://doi.org/10.1109/ISBI.2018.8363547
47. Atanassov KT. Intuitionistic fuzzy sets. Fuzzy sets Syst. 1986;20(1):87–96.
48. Mendonca T, Celebi M, Mendonca T, Marques J. Ph2: A public database for the analysis of dermoscopic images. Dermosc. Image Anal. 2015
49. Codella N.C, Gutman D, Celebi M.E, Helba B, Marchetti M.A, Dusza S.W, Kalloo A, Liopyris K, Mishra N, Kittler H, et al. Skin lesion analysis toward melanoma detection: a challenge at the 2017 international symposium on biomedical imaging (isbi), hosted by the international skin imaging collaboration (isic). In: 2018 IEEE 15th International Symposium on Biomedical Imaging (ISBI 2018), 2018;pp. 168–172. IEEE
50. Tschandl P, Rosendahl C, Kittler H. The ham10000 dataset, a large collection of multi-source dermatoscopic images of common pigmented skin lesions. Sci Data. 2018;5(1):1–9.
51. Silva V.D. Finding dominant peaks and valleys of an image histogram 2020. https://www.mathworks.com/matlabcentral/fileexchange/31570-finding-dominant-peaks-and-valleys-of-an-image-histogram
52. Chaira T. A rank ordered filter for medical image edge enhancement and detection using intuitionistic fuzzy set. Appl Soft Comput. 2012;12(4):1259–66.
53. Verma H, Agrawal R, Sharan A. An improved intuitionistic fuzzy c-means clustering algorithm incorporating local information for brain image segmentation. Appl Soft Comput. 2015;46:543–57.
54. Pham DL. Spatial models for fuzzy clustering. Comput Vis Image Underst. 2001;84(2):285–97.
55. Bezdek JC, Ehrlich R, Full W. Fcm: the fuzzy c-means clustering algorithm. Comput Geosci. 1984;10(2–3):191–203.
56. Namburu A, Kumar Samay S, Edara SR. Soft fuzzy rough set-based mr brain image segmentation. Appl Soft Comput. 2017;54:456–66.
57. Tou JT, Gonzalez RC. Pattern recognition. Reading: Addison-Wesley; 1974.
58. Maji P, Pal SK. Rfcm: a hybrid clustering algorithm using rough and fuzzy sets. Fund Inform. 2007;80(4):475–96.
59. Garcia-Arroyo JL, Garcia-Zapirain B. Segmentation of skin lesions in dermoscopy images using fuzzy classification of pixels and histogram thresholding. Comput Methods Prog Biomed. 2019;168:11–9.